


# Oxygen extraction efficiency and white matter lesion burden in older adults exhibiting radiological evidence of capillary shunting

Journal of Cerebral Blood Flow & Metabolism  
 2022, Vol. 42(10) 1933–1943  
 © The Author(s) 2022  
 Article reuse guidelines:  
 sagepub.com/journals-permissions  
 DOI: 10.1177/0271678X221105986  
 journals.sagepub.com/home/jcbfm



Meher R Juttukonda<sup>1,2</sup>, Kimberly A Stephens<sup>1</sup>, Yi-Fen Yen<sup>1,2</sup>,  
 Casey M Howard<sup>1</sup>, Jonathan R Polimeni<sup>1,2,3</sup> ,  
 Bruce R Rosen<sup>1,2,3</sup> and David H Salat<sup>1,2,4</sup>

## Abstract

White matter lesions (WML) have been linked to cognitive decline in aging as well as in Alzheimer's disease. While hypoperfusion is frequently considered a cause of WMLs due to the resulting reduction in oxygen availability to brain tissue, such reductions could also be caused by impaired oxygen exchange. Here, we tested the hypothesis that venous hyperintense signal (VHS) in arterial spin labeling (ASL) magnetic resonance imaging (MRI) may represent a marker of impaired oxygen extraction in aging older adults. In participants aged 60–80 years ( $n = 30$ ), we measured cerebral blood flow and VHS with arterial spin labeling, maximum oxygen extraction fraction ( $OEF_{max}$ ) with dynamic susceptibility contrast, and WML volume with  $T_1$ -weighted MRI. We found a significant interaction between  $OEF_{max}$  and VHS presence on WML volume ( $p = 0.02$ ), where lower  $OEF_{max}$  was associated with higher WML volume in participants with VHS, and higher  $OEF_{max}$  was associated with higher WML volume in participants without VHS. These results indicate that VHS in perfusion-weighted ASL data may represent a distinct cerebrovascular aging pattern involving oxygen extraction inefficiency as well as hypoperfusion.

## Keywords

Aging, capillary shunting, cerebral blood flow, oxygen extraction fraction, white matter lesions

Received 14 January 2022; Revised 19 April 2022; Accepted 14 May 2022

## Introduction

White matter lesions (WMLs) are a common manifestation of cerebral small vessel disease,<sup>1</sup> and the presence of these lesions has been linked to declining cognitive function in aging as well as in patients with Alzheimer's disease and related dementias.<sup>2–8</sup> While the etiology of these lesions is often presumed to be vascular in nature,<sup>9,10</sup> microvascular hemodynamic mechanisms associated with the formation and progression of these lesions are highly complex and remain incompletely understood. Thus, there is an urgent need to improve our understanding of these mechanisms so that therapies aimed at preventing or delaying WML-related cognitive decline may be developed and titrated to high-risk individuals.

Noninvasive magnetic resonance imaging (MRI) techniques including arterial spin labeling (ASL)<sup>11</sup>

have frequently been used to study how cerebral blood flow (CBF) changes with aging.<sup>12–17</sup> In pseudo-continuous ASL,<sup>18</sup> the magnetization of arterial blood water in the neck is inverted (i.e., labeled) using a long chain of radiofrequency pulses. After

<sup>1</sup>Athinoula A. Martinos Center for Biomedical Imaging, Department of Radiology, Massachusetts General Hospital, Charlestown, MA, USA

<sup>2</sup>Department of Radiology, Harvard Medical School, Boston, MA, USA

<sup>3</sup>Division of Health Sciences and Technology, Harvard-Massachusetts Institute of Technology, Cambridge, MA, USA

<sup>4</sup>Neuroimaging Research for Veterans Center, VA Boston Healthcare System, Boston, MA, USA

## Corresponding author:

Meher R Juttukonda, 149 Thirteenth Street, Suite 2301, Charlestown, MA 02129, USA.

Email: mjuttukonda@mgh.harvard.edu

a post-labeling delay to allow this labeled blood to reach and perfuse tissue, MR images of a volume containing the brain are acquired. These 'label' images are subtracted from 'control' images acquired without labeling to yield perfusion-weighted images that are converted to CBF using a kinetic model.<sup>19</sup>

While ASL has proven difficult for measuring perfusion in white matter, gray matter CBF has been extensively studied as a biomarker in various diseases. Using ASL or other MRI approaches, overwhelming evidence has been presented that cerebral perfusion decreases with increasing age and represents a marker of aging-related hemodynamic impairment.<sup>13,20,21</sup> Therefore, WML formation and progression has been frequently attributed to aging-related hypoperfusion or impairment in the regulation of CBF.<sup>22</sup> However, perfusion represents only one component of the equation that governs the relationship between cerebral oxygen supply and demand:

$$CMR_{O_2} = CBF \cdot Hb \cdot Y_a \cdot OEF \quad (1)$$

where  $CMR_{O_2}$  is the cerebral metabolic rate of oxygen consumption,  $CBF$  is the perfusion,  $Hb$  is the concentration of hemoglobin in blood,  $Y_a$  is the oxygen saturation of hemoglobin, and  $OEF$  is the tissue oxygen extraction fraction (i.e., the ratio of oxygen consumed to oxygen delivered). The offloading of oxygen from capillaries into brain tissue is a passive process governed in part by the concentration gradient of oxygen in the two compartments. Recent work has shown that capillary flow patterns also contribute to the efficiency at which oxygen is offloaded into tissue.<sup>23</sup> The maximum OEF ( $OEF_{max}$ ) is defined as an upper bound for OEF determined by the capillary mean transit time and transit heterogeneity for a given tissue oxygen tension.<sup>24</sup> While prior work has characterized the effect of age on CBF and OEF, less is known regarding how  $OEF_{max}$  is affected by aging and how it may be associated with WML pathophysiology.

Recently, venous hyperintense signal (VHS) in perfusion-weighted ASL images has been characterized as a marker of capillary shunting and reduced OEF in young adults with sickle cell anemia.<sup>25,26</sup> In the absence of pathology affecting microvascular flow, it is expected that labeled arterial blood water arrives in the capillary bed and exchanges sufficiently with tissue water, resulting in outflow into veins that contains a good mixture of labeled and unlabeled spins. Therefore, little to no ASL difference signal is expected to be present in large veins. However, in the presence of disturbed microvascular flow, it is possible that labeled blood water passes through the capillaries and into the venous system too quickly to allow for good mixing

with tissue water. In this case, the presence of labeled arterial blood causes bright signal to appear inside of large draining veins (Figure 1). Since the efficiency of oxygen exchange in the capillaries is dependent in part on these microvascular transit times, we posited that the presence of VHS could be indicative of oxygen exchange efficiency.

Prior studies in young anemic adults have shown that the presence of VHS was indicative of reduced OEF and could be associated with elevated risk for silent lesions.<sup>26</sup> Interestingly, such relationships were also observed, but at a lower prevalence, in young adults who were not anemic but exhibited radiological evidence of WMLs.<sup>26</sup> In the present study, we extended this work to investigate whether VHS may also be present in older adults and whether it may represent a more general marker of hemodynamic impairment associated with oxygen extraction efficiency in an aging population. Based on prior findings in young adults, we hypothesized that older adults with VHS would exhibit impaired  $OEF_{max}$  and elevated burden of WMLs compared to those without VHS.

## Methods

### Study design and participants

All components of this study were performed in compliance with the ethical standards instituted by the Mass General Brigham Research Compliance office and as set forth by the Belmont Report. Older adult volunteers (60–80 years of age) were recruited through the Brain Aging and Dementia Laboratory at Massachusetts General Hospital and provided informed written consent as part of this Mass General Brigham Institutional Review Board-approved study (IRB #2013P001639). Exclusion criteria included major neurological or psychiatric disorders, including dementia or clinical stroke, as well as the presence of substantial systemic illnesses likely to confound the study. Participants underwent two imaging sessions: a non-contrast MRI scan at 3 Tesla (3T; Siemens Biograph mMR) and a contrast-enhanced MRI scan at 7 Tesla (7T; Siemens Magnetom). A battery of neuropsychological testing, including the Montreal Cognitive Assessment (MoCA), was administered to measure overall cognitive health as previously described,<sup>27</sup> and participants were classified as exhibiting mild cognitive impairment (MCI) based on performance falling one standard deviation or more below published normative values on at least two cognitive domains.<sup>28</sup> Of note, only data from participants who underwent both imaging sessions were included in this retrospective study.

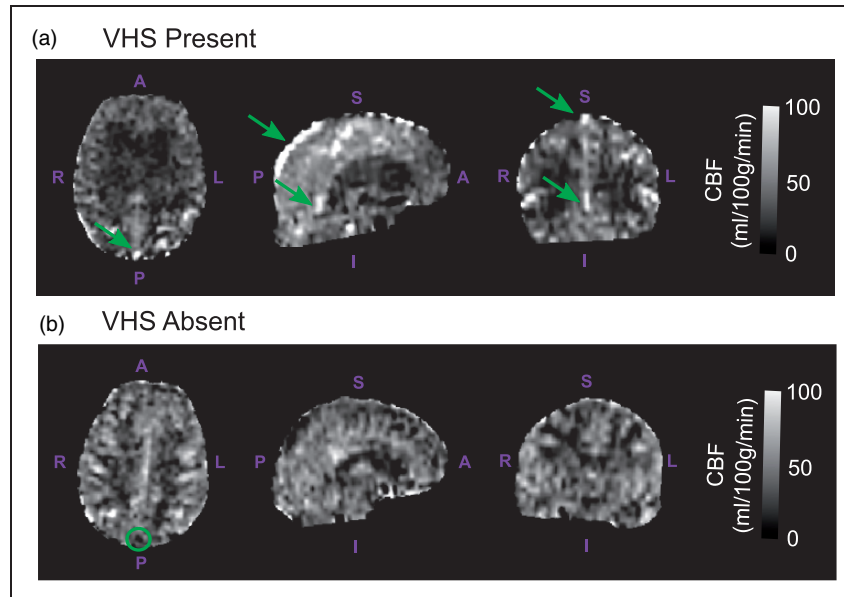


**Figure 1.** Venous hyperintense signal: cerebral blood flow (CBF)-weighted images derived with arterial spin labeling (ASL) were assessed for venous hyperintense signal (VHS). Representative axial, sagittal, and coronal CBF images (from left to right) are shown here for individuals with VHS present (a; VHS+; 79 y.o. female) and VHS absent (b; VHS–; 64 y.o. female). Participants were classified as VHS+ if bright signals were contiguously observed at locations where large draining veins, including the superior sagittal sinus and straight sinus, are expected to be present (green arrows). Images where no signal enhancement was observed relative to surroundings in such regions (green circle) were classified as VHS–.

### Image acquisition

$T_1$ -weighted MR images were acquired at 3T using a multi-echo magnetization-prepared rapid gradient echo (ME-MPRAGE) sequence (repetition time [TR] = 2530 ms; inversion time [TI] = 1100 ms; echo times [TE] = 1.69 ms, 3.55 ms, 5.41 ms, and 7.27 ms; flip angle =  $7^\circ$ ; spatial resolution =  $1.0 \times 1.0 \times 1.0 \text{ mm}^3$ ). The individual echoes were combined by using a root mean square to generate a single  $T_1$ -weighted volume for tissue segmentation and image registration. Fluid-attenuated-inversion-recovery (FLAIR)  $T_2$ -weighted MR images were also acquired at 3T (TR = 5000 ms; TE = 400 ms; flip angle =  $120^\circ$ ; spatial resolution =  $0.5 \times 0.5 \times 1.0 \text{ mm}^3$ ).

ASL MR images were acquired at 3T with pseudo-continuous labeling (total labeling duration = 1500 ms and post-labeling delay = 1200 ms) and without background or vascular suppression using a 2D echo planar imaging readout (TR = 4000 ms; TE = 12 ms; spatial resolution =  $3.5 \times 3.5 \times 5.0 \text{ mm}^3$ ; control/label pairs = 40).

Dynamic susceptibility contrast (DSC) MRI data were acquired at 7T with gadolinium contrast. A bolus of 0.2 ml/kg (0.1 mmol/kg) of gadopentetate dimeglumine (MAGNEVIST, Bayer Healthcare) was administered intravenously at a constant rate between 1.0–2.0 ml/s, followed by a saline flush at the same rate. A 2D single-shot gradient-echo echo planar imaging sequence was used for the readout (TR = 1500 ms;

TE = 22 ms; flip angle =  $75^\circ$ ; spatial resolution =  $1.5 \times 1.5 \times 1.5 \text{ mm}^3$ ; nominal echo spacing = 0.69 ms; Generalized Auto-calibrating Partially Parallel Acquisition factor = 3; multi-band factor = 2). A total of 100 frames were collected.

### Structural image processing

$T_1$ -weighted images were automatically processed to reconstruct cortical surfaces and to segment volume regions-of-interest using the Freesurfer ‘recon-all’ procedure.<sup>29,30</sup> Segmentation of these images using a watershed/surface deformation procedure and automatically registered into a common surface template using a surface-based averaging technique by considering cortical folding patterns.<sup>31</sup> A pre-defined gray matter mask in the standard space was then inversely mapped to each participant’s native space using a high-dimensional spherical morphing procedure to define gray matter masks in each participant’s images. WML volumes were calculated using  $T_1$ -weighted images with the FreeSurfer-based procedure for measuring white matter hypointensities as described previously.<sup>2</sup>

### Physiological image processing

ASL images from each participant were motion-corrected<sup>32</sup> and pair-wise subtracted.<sup>33</sup> CBF was then

computed using a two-compartment kinetic model as previously described.<sup>34</sup>

$$CBF = \frac{6000 \cdot \lambda \cdot \Delta M \cdot \exp\left(\frac{d}{T_{1,a}}\right)}{2 \cdot \alpha \cdot M_0 \cdot T_{1,a} \cdot \left[ \exp\left(-\frac{\max(PLD-d,0)}{T_{1,t}}\right) - \exp\left(-\frac{\max(\tau + PLD - d, 0)}{T_{1,t}}\right) \right]} \quad (2)$$

where  $\lambda$  ( $=0.9$  g/ml) is the blood-brain partition coefficient,  $\Delta M$  is the ASL difference signal in each voxel,  $\alpha$  ( $=0.85$ ) is the labeling efficiency,  $M_0$  is the equilibrium magnetization in each voxel,  $T_{1,a}$  ( $=1.65$  s) is the longitudinal relaxation of arterial blood,  $T_{1,t}$  ( $=1.2$  s) is the longitudinal relaxation time of gray matter,  $PLD$  is the post-labeling delay (after slice-timing correction),  $\tau$  ( $=1.5$  s) is the labeling duration, and  $\delta$  ( $=1.52$  s) is the ATT chosen as the mean gray matter ATT previously observed in a similar age range.<sup>14</sup>  $M_0$  represents the equilibrium magnetization image, which was estimated using a scaling of the mean control image.<sup>19</sup> This image was then aligned with corresponding  $T_1$ -weighted images using a boundary-based registration algorithm,<sup>31</sup> and this transform was applied to corresponding CBF images to enable quantitation in a whole gray matter region-of-interest. CBF images from each participant were also qualitatively assessed for the presence (VHS+) or absence (VHS-) of labeled blood inside of large draining veins, including the superior sagittal sinus, inferior sagittal sinus, and straight sinus, in a similar manner as a previously established procedure with high inter-rater reliability.<sup>25</sup> More specifically, a participant was classified as being VHS+ if the presence of bright signal was observed in at least one of these three vessels and VHS- if no labeled blood was detectable in any of these vessels.

DSC-MRI data were motion-corrected<sup>32</sup> and processed using the Penguin/pgui software to convert the  $T_2^*$  signal time curves of each voxel to contrast concentration time curves.<sup>35</sup> An arterial input function (AIF) from middle cerebral artery branches was selected by the software based on cluster analysis of voxel-wise dynamic curves.<sup>36</sup> The AIF was then used in a vascular model developed by Ostergaard et al.<sup>24,35,37</sup> to derive perfusion parametric maps, including the  $OEF_{max}$  images. DSC-MRI data were aligned within-subject to corresponding  $T_1$ -weighted images using a boundary-based registration algorithm,<sup>31</sup> and this transform was applied to corresponding  $OEF_{max}$  images to enable quantitation in a similar gray matter region-of-interest, as with CBF. DSC data were also used to derive other parameters, including mean transit

time, CBF, and cerebral blood volume. Analyses with these parameters as a function of VHS presence are presented as supplementary information.

### Statistics

Continuous variables are described with the corresponding median and interquartile range, and prevalence measures are described with percentages. All statistical analysis was performed using two-tailed tests when applicable and at a 0.05 level of significance. Continuous variables were assessed for normality using Shapiro-Wilk tests.

The primary statistical objective of this study was to test the hypothesis that older age is associated with lower  $OEF_{max}$  and elevated WML volume in VHS+ versus VHS- participants. First, we assessed associations between CBF and age and between  $OEF_{max}$  and age using Spearman's correlation analysis. To study the effect of VHS presence, we then performed linear regressions with the inclusion of a term modeling the interaction between VHS and age on each of CBF and  $OEF_{max}$  separately. Second, we assessed whether WML volume was different between VHS+ and VHS- participants using a two-tailed Wilcoxon rank-sum test. We then assessed between WML volume and age using Spearman's correlation analysis followed by a linear regression modeling the interaction between VHS and age on WML volume. Finally, we assessed the relationships between CBF and WML volume and between  $OEF_{max}$  and WML volume using Spearman's correlation analysis. We also performed linear regressions modeling the interaction between VHS and each of CBF and  $OEF_{max}$  on WML volume separately.

## Results

### Demographics and prevalence of venous hyperintense signal

A total of 30 individuals satisfied the inclusion criteria for this study. Demographic information, cognitive data, and vascular risk factor prevalence from these participants are shown in Table 1. Overall, ten participants (33%) exhibited neuropsychologically-defined criteria for MCI.

Overall, VHS was present in 30.0% of participants (9/30). Participants with VHS (median age = 70 years) were older than those without VHS (median age = 65 years), but this difference was not statistically significant ( $p=0.18$ ). There was no significant difference in the male-to-female ratio in the groups with VHS (33% male) and without VHS (52% male;  $p=0.34$ ).

Of the continuous variables presented below, age ( $p=0.02$ ) and WML volume ( $p<0.01$ ) were normally

**Table 1.** Participant demographics, cognitive scores, and vascular risk factor prevalence.

	Overall (n = 30)	VHS (n = 9)	No VHS (n = 21)	p-value
Age	Median: 67 years IQR: 62–70 years	Median: 70 years IQR: 64–71 years	Median: 65 years IQR: 62–70 years	0.18
Sex	Male = 14 Female = 16	Male = 3 Female = 6	Male = 11 Female = 10	0.34
MoCA	Median: 26 IQR: 23–28	Median: 28 IQR: 27–30	Median: 25 IQR: 23–27	0.01
Hypertension	10%	22%	5%	0.14
Diabetes	3%	11%	0%	0.12
Hyperlipidemia	7%	11%	5%	0.52

MoCA: Montreal Cognitive Assessment; IQR: interquartile range; VHS: venous hyperintense signal. p-values are for comparisons between groups with versus without VHS.

distributed while CBF ( $p=0.22$ ) and  $OEF_{max}$  ( $p=0.67$ ) were not.

**Cerebrovascular physiology.** Age was not correlated with ASL-derived gray matter CBF ( $\rho = -0.08$ ;  $p=0.68$ ), and there was no interaction between age and VHS presence when examining the association with CBF (Figure 2(a);  $p=0.58$ ). Supplementary analyses examining correlations between DSC- and ASL-derived CBF measures showed that these measures may be correlated in individuals without VHS but not in those with VHS (Supplementary Figure 1).

There was no relationship between  $OEF_{max}$  and age overall ( $\rho = 0.24$ ;  $p=0.21$ ), but there was a significant interaction between age and VHS presence ( $p < 0.01$ ). More specifically, older age is associated with higher  $OEF_{max}$  in participants without VHS, while older age is associated with lower  $OEF_{max}$  in participants with VHS (Figure 2(b)).

**White matter lesion volume.** Overall, participants with VHS (median volume = 4146 mm<sup>3</sup>) did not exhibit a significantly greater WML burden compared to those without VHS (median volume = 2548 mm<sup>3</sup>;  $p=0.18$ ; Figure 3(a)). However, older age is significantly correlated with higher WML volume ( $\rho = 0.46$ ;  $p=0.01$ ), and there was a significant interaction between age and VHS presence when examining the association with WML volume ( $p=0.04$ ), with VHS+ individuals displaying a steeper increase of WML volume with increasing age (Figure 3(b)).

WML volume was not significantly correlated with CBF ( $\rho = -0.21$ ;  $p=0.26$ ), and there was no interaction between CBF and VHS presence when examining the association with WML volume ( $p=0.86$ ; Figure 4 (a)). There was no relationship between  $OEF_{max}$  and WML volume ( $\rho = -0.01$ ;  $p=0.95$ ) overall, but there was a significant interaction between  $OEF_{max}$  and VHS presence ( $p=0.02$ ). More specifically, lower  $OEF_{max}$  was associated with higher WML volume in

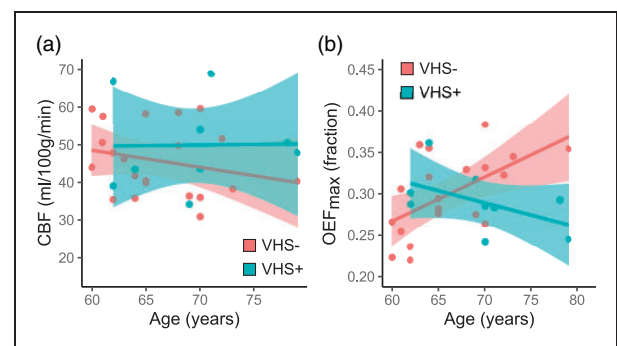


**Figure 2.** Age and hemodynamic physiology: There was no significant interaction between age and venous hyperintense signal (VHS) presence (VHS+) or absence (VHS-) on the association between cerebral blood flow (CBF) and age (a) and There was a significant interaction between age and VHS on maximum oxygen extraction fraction ( $OEF_{max}$ ), with older age associated with higher  $OEF_{max}$  in VHS- participants and lower  $OEF_{max}$  in VHS+ participants (b).

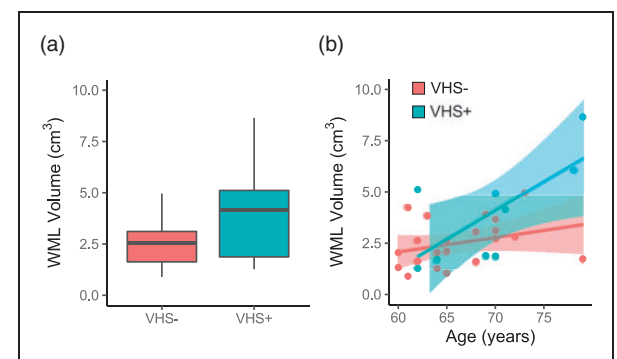


**Figure 3.** Age and white matter lesion volume: Overall, participants with VHS (VHS+) did not exhibit a significantly higher white matter lesion (WML) volume compared to participants without VHS (VHS-) (a) and However, there was a significant interaction between age and VHS on WML volume, with older age associated with a higher WML volume in VHS+ compared to VHS- participants (b).

participants with VHS, while higher  $OE_{max}$  was associated with higher WML volume in participants without VHS (Figure 4(b)).

Outputs from regression analyses reported above are summarized in Table 2. Representative examples of participants with and without VHS (Figure 5) demonstrate that these group-level findings can also be observed at the individual level. Analyses conducted with other DSC-based measures, including mean transit time and cerebral blood volume, are shown in Supplementary Figure 2.

## Discussion

In this study, we characterized a novel imaging marker of oxygen extraction inefficiency and its relationship

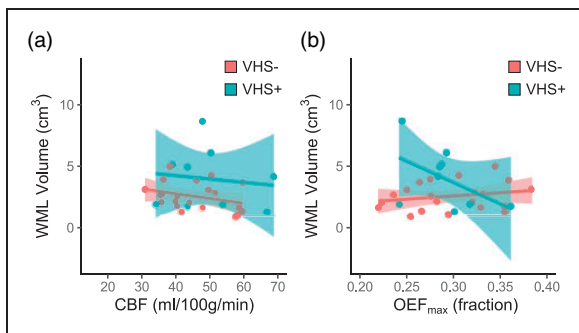


**Figure 4.** White matter lesion volume and hemodynamic physiology. There was no significant interaction between cerebral blood flow (CBF) and venous hyperintense signal (VHS) presence (VHS+) or absence (VHS-) on white matter lesion (WML) volume (a). However, there was a significant interaction between maximum oxygen extraction fraction ( $OE_{max}$ ) and VHS on WML volume, with lower  $OE_{max}$  associated with higher WML volume in VHS+ participants and lower WML volume in VHS- participants (b).

with age, cerebral hemodynamic physiology, and white matter lesion burden in a cohort of older adults between 60–80 years of age. We used ASL to assess for CBF and for venous signal indicative of capillary shunting and DSC to compute  $OE_{max}$  as a measure of oxygen exchange efficiency. Our main findings were that VHS was prevalent in 30% of our sample of older adults, and participants with VHS were older (median age = 70 years) compared to participants without VHS (median age = 65 years). While not significantly related to CBF, the relationship between age and  $OE_{max}$  was dependent on VHS presence, with lower  $OE_{max}$  corresponding to older age when VHS was present. Finally, higher WML volumes were correlated with lower  $OE_{max}$  in participants with VHS but not in those without VHS. These results indicate that the presence of VHS on perfusion-weighted ASL data could serve as a marker of a distinct cerebrovascular aging pattern that potentially involves physiological mechanisms involving oxygen extraction inefficiency.

The relationship between oxygen demand and oxygen supply in the brain can be described using Fick's first law, where the cerebral metabolic rate of oxygen consumption is supported by the product of CBF and  $OE_{max}$ .<sup>38</sup> Prior studies that have included a wide age range of participants have shown decreases in CBF with aging,<sup>39–41</sup> but relatively few have included participants older than 60 years. Those that include individuals between 60–80 years suggest a weaker association with age and higher variability during these two decades.<sup>40,42–44</sup> Additionally, lower CBF was shown to be associated with greater severity of periventricular hyperintensities, which is also suggested by our comparisons in individuals with and without VHS. However, the relationship between  $OE_{max}$  and severity was not as clear, with the highest severity group displaying lower  $OE_{max}$  than the moderate severity group.<sup>45</sup>

**Table 2.** Coefficients and p-values of terms from the multivariate regression analyses.

	Intercept	Age	VHS	Interaction
CBF	75.3 $p = 0.02^*$	−0.449 $p = 0.34$	−27.8 $p = 0.59$	0.481 $p = 0.52$
$OE_{max}$	−0.00419 $p = 0.73$	0.00512 $p < 0.01^*$	0.536 $p = 0.01^*$	−0.00806 $p < 0.01^*$
WML volume	−2037 $p = 0.62$	69 $p = 0.27$	−13611 $p = 0.05^*$	213 $p = 0.04^*$
	Intercept	CBF	VHS	Interaction
WML volume	4306 $p = 0.03^*$	−39 $p = 0.34$	1013 $p = 0.75$	12 $p = 0.86$
	Intercept	$OE_{max}$	VHS	Interaction
WML volume	977 $p = 0.65$	5236 $p = 0.47$	13137 $p = 0.01^*$	−40188 $p = 0.02^*$

\*Represents statistically significant regression parameters.

CBF: cerebral blood flow;  $OE_{max}$ : maximum oxygen extraction fraction; VHS: venous hyperintense signal; WML: white matter lesions.

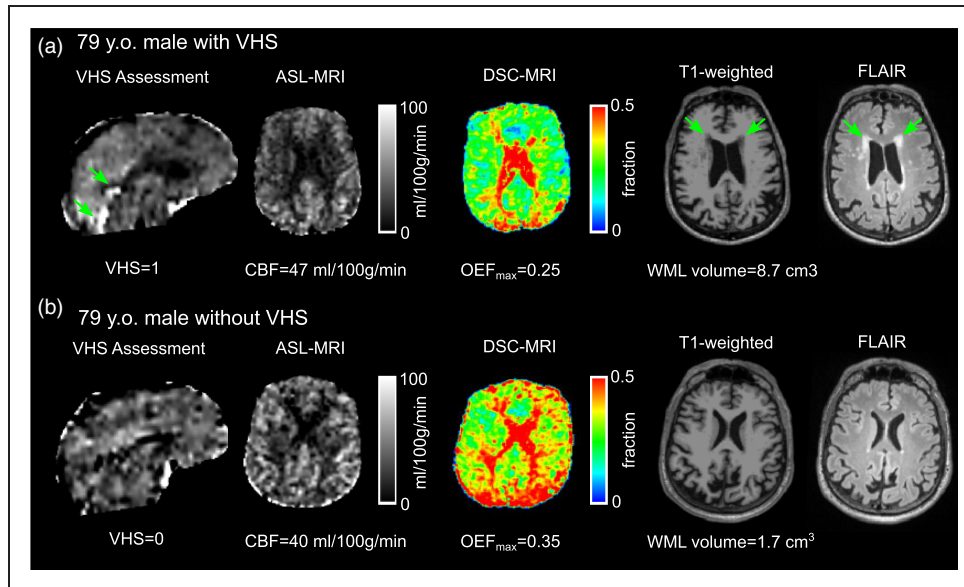


**Figure 5.** Representative examples: Venous hyperintense signal (VHS) assessment, cerebral blood flow (CBF), maximum oxygen extraction fraction ( $OE_{max}$ ), T<sub>1</sub>-weighted, and T<sub>2</sub>-weighted fluid-attenuated inversion recovery (FLAIR) MR images are shown for two representative participants matched for age and sex but differing by the presence of VHS. CBF exhibited a small difference between the participant with (a) versus without VHS (b), but  $OE_{max}$  was markedly lower in the participant with VHS, and white matter lesion (WML) volume was much higher in the participant with VHS. As a note, T<sub>1</sub>-weighted images were used for WML volume quantification, while T<sub>2</sub>-FLAIR images are shown here for visualization of the lesions.

From our understanding of ischemic disease, it is thought that  $OE_{max}$  should increase as CBF decreases to maintain  $CMR_{O_2}$ .<sup>46,47</sup> In the presence of disturbed capillary flow patterns, however, it may no longer be possible for this relationship to persist due to resulting impairment in oxygen extraction efficiency.<sup>48</sup> It has been previously shown that  $OE_{max}$  is limited by capillary flow patterns,<sup>23</sup> and faster transit across the capillary bed with aging or disease could result in a decrease in  $OE_{max}$ . While such a gradual decrease may first result in compensatory increases in CBF, sufficient oxygen extraction may only be maintained after a certain threshold only if CBF is suppressed to prolong capillary transit times.<sup>49</sup> This mismatch may in turn result in a chronic imbalance between oxygen demand and supply and elevated levels of hypoxic insult presenting as higher WML volumes. However, the degree to which this phenomenon is present and associated with white matter lesions is not yet fully understood. In this study, we implemented an approach that uses DSC MRI to calculate  $OE_{max}$ . While these methods were developed for use at 3T, they assume a linear relationship between contrast agent concentration and changes in tissue and blood water relaxation rates and should be equally applicable at 7T.

Our experimental results closely match these theoretical expectations regarding the relationship between aging,  $OE_{max}$ , and WML volumes. The lack of an expected relationship between CBF and age could be

related to the narrow age range studied coupled with relatively small sample size. Meanwhile, we found that  $OE_{max}$  decreases with increasing age in participants with VHS but increases with older age in participants without VHS. Prior studies in healthy adults have described a steady decrease in venous oxygenation with advancing age, implying that  $OE_{max}$  increases with age, across the adult lifespan.<sup>41</sup> However, our results indicate that there is heterogeneity in the directionality of the relationship between age and  $OE_{max}$ , which may be described by the presence or absence of VHS physiology. Our analyses examining the relationship between hemodynamics and WML volumes provided a very similar result. Higher WML volumes were associated with lower  $OE_{max}$  in VHS+ participants and with higher  $OE_{max}$  in VHS- participants. Taken together, these could indicate that VHS may be indicative of impairment in oxygen exchange, which could lead to greater WML burden with aging.

Venous signals in perfusion-weighted MRI acquired with ASL were first characterized as markers of oxygen extraction efficiency in young adults (aged 16–39 years) with sickle cell anemia.<sup>25</sup> In this patient population,  $OE_{max}$  was shown to be lower when VHS was present in patients with a history of silent infarcts or white matter lesions.<sup>26</sup> The rationale for capillary flow disruptions leading to tissue hypoxia in this disease where high flow has been demonstrated has been previously described.<sup>50</sup> While the labeling durations (1000 ms vs.

1500 ms) and post-labeling delays (1900 ms vs. 1200 ms) of the ASL sequences used in the two studies are different, the time since the start of labeling (i.e., the sum of the labeling duration and the post-labeling delay) is similar (2900 ms vs. 2700 ms). For VHS-related considerations, this is the quantity of importance since the difference between start of labeling and the time of imaging places a limit on how short the sum of the arterial transit time and capillary transit time must be for labeled blood water to be detected in the veins. We have recently shown that arterial transit times in adults between 60–80 years of age are  $\sim 1.5$  s,<sup>14</sup> and typical capillary transit times are thought to be  $\sim 2$  s. Therefore, in the absence of pathology, we expect that the shortest imaging time at which labeled signal should be detectable is at least  $\sim 3.5$  s. This estimate does not include the time necessary for the labeled blood to travel the venous system to the draining veins, but including this time would only increase this lower limit. However, venous signals in this study were observed at just 2.7 s following the start of labeling, indicating that either the arterial transit time and/or the capillary transit time must be reduced in participants with VHS. Our prior work showing strong increases in arterial transit times with increasing age<sup>14</sup> leads us to therefore posit that VHS is likely due to reduced capillary transit times. Supplementary analyses indeed indicate that capillary mean transit time may also decrease with age in VHS+ individuals (Supplementary Figure 2), but further studies are necessary to confirm this hypothesis. Importantly, only venous signal apparent when using asymmetric labeling schemes (versus symmetric or non-selective labeling) may be interpreted as microvascular transit related since the spin labeling occurs in cervical arteries of the neck and not in the brain. In addition, this phenomenon is distinct from arteriovenous malformations, which result in physical shunts and may also play a role in white matter lesion pathophysiology.<sup>51</sup>

### Limitations

Our results should be considered in the context of the following limitations. First, our sample size ( $n=30$  participants) is modest, limiting our ability to generalize the findings from the data. Second, while the timing of our ASL acquisition may be particularly well-suited for studying capillary flow disturbances, the post-labeling delay (=1200 ms) is shorter than what has been recently recommended for using in older adults<sup>19</sup> due to the onset of this study in 2014 prior to wide dissemination of these recommendations. The use of a shorter delay time could introduce arterial transit time as a potential confounding factor into our CBF measures as transit times are known to

increase with age. However, this is somewhat mitigated by our use of a 2D echo planar readout and an ascending slice progression for the ASL acquisition, since the effective post-labeling increases for each slice and reaches  $\sim 1500$  ms for the most superior slices. While DSC can also provide a measure of CBF, this measure was not used as the primary CBF parameter in this study to avoid the potential for correlated effects with  $OEF_{\max}$ . However, as illustrated in Supplementary Figure 3, CBF in WM also indicates differences in hemodynamic relationships based on VHS presence. Third,  $OEF_{\max}$  represents only the theoretical upper bound and does not provide a measure of the true OEF of brain tissue. While there are elegant MRI-based approaches available for measuring  $OEF_{\max}$ , this parameter was not of primary interest in the study for which these data were acquired. However, ongoing work aims to utilize such approaches to address this issue. Fourth, while our structural marker of interest (WML volume) is a quantity belonging to white matter, our physiological measurements were made in gray matter. ASL in white matter is inherently more difficult due to much lower blood volumes and much longer transit times compared to gray matter. While we have recently shown that these limitations may be overcome with state-of-the-art sequences and updated processing schemes,<sup>14</sup> ASL data used in this study were acquired prior to the implementation of these more recently developed innovations. Fifth, our measure of VHS is currently a qualitative one, but ongoing work involves the development of a multiple post-labeling delay approach for automatically detecting and quantifying venous ASL signal. Such an approach would also allow for estimation of arterial transit times as well as a more robust computation of CBF. Finally, while large vessel disease has been shown to influence microvascular hemodynamics, magnetic resonance angiography data were not acquired as part of this study. Therefore, it was not possible to determine the degree to which these large vessel effects could be present. However, none of the participants included in this study exhibited a history of stroke.

### Conclusions

In conclusion, we have characterized the presence of labeled arterial blood water in large draining veins (i.e., capillary shunting) as a potential noninvasive mechanism contributing to reduced oxygen availability to the brain with aging. Using independent measures of VHS (with ASL),  $OEF_{\max}$  (with DSC), and WML volume (with  $T_1$ -weighted imaging), we have shown that the presence of venous signals in perfusion-weighted ASL MRI may be indicative of oxygen extraction inefficiency-related impairment with aging.



However, as the physiology underlying these lesions is highly complex, future work is required to understand how VHS and capillary hemodynamics may interact with different risk factors for WMLs and AD to influence progression of these lesions, how they may be associated with measures of cognitive function, and potential regional differences in physiology based on vessel-specific presence of VHS.

### Funding

The author(s) disclosed receipt of the following financial support for the research, authorship, and/or publication of this article: This work was supported by the National Institutes of Health (R01NR010827) and the American Heart Association (19CDA34790002).

### Acknowledgements

We would like to thank Dr. Leif Ostergaard for helpful discussions regarding the applicability of 7T dynamic susceptibility contrast approaches for quantifying hemodynamic parameters relevant to this study.

### Declaration of conflicting interests

The author(s) declared no potential conflicts of interest with respect to the research, authorship, and/or publication of this article.

### Authors' contributions

Meher R. Juttukonda: Involved in study conception and design; analysis and interpretation of data; manuscript drafting and revision. Kimberly A. Stephens: Involved in data acquisition; analysis and interpretation of data; manuscript revision; Yi-Fen Yen: Involved in analysis and interpretation of data; manuscript revision. Casey M. Howard: Involved in data acquisition; manuscript revision. Jonathan R. Polimeni: Involved in data acquisition; manuscript revision; Bruce R. Rosen: Involved in analysis and interpretation of data; manuscript revision; David H. Salat: Involved in study conception and design; analysis and interpretation of data; manuscript revision.

### ORCID iD

Jonathan R Polimeni  <https://orcid.org/0000-0002-1348-1179>

### Supplemental material

Supplemental material for this article is available online.

### References

1. Wardlaw JM, Smith C and Dichgans M. Small vessel disease: mechanisms and clinical implications. *Lancet Neurol* 2019; 18: 684–696.
2. Coutu JP, Goldblatt A, Rosas HD, et al. White matter changes are associated with ventricular expansion in aging, mild cognitive impairment, and Alzheimer's disease. *J Alzheimers Dis* 2016; 49: 329–342.
3. Graff-Radford J, Arenaza-Urquijo EM, Knopman DS, et al. White matter hyperintensities: relationship to amyloid and tau burden. *Brain* 2019; 142: 2483–2491.
4. Lee S, Viqar F, Zimmerman ME, et al. White matter hyperintensities are a core feature of Alzheimer's disease: evidence from the dominantly inherited Alzheimer network. *Ann Neurol* 2016; 79: 929–939.
5. Carmichael O, Schwarz C, Drucker D, Alzheimer's Disease Neuroimaging Initiative, et al. Longitudinal changes in white matter disease and cognition in the first year of the Alzheimer disease neuroimaging initiative. *Arch Neurol* 2010; 67: 1370–1378.
6. Yoshita M, Fletcher E, Harvey D, et al. Extent and distribution of white matter hyperintensities in normal aging, MCI, and AD. *Neurology* 2006; 67: 2192–2198.
7. Lindemer ER, Greve DN, Fischl BR, et al. Regional staging of white matter signal abnormalities in aging and Alzheimer's disease. *Neuroimage Clin* 2017; 14: 156–165.
8. Provenzano FA, Muraskin J, Tosto G, Alzheimer's Disease Neuroimaging Initiative, et al. White matter hyperintensities and cerebral amyloidosis: necessary and sufficient for clinical expression of Alzheimer disease? *JAMA Neurol* 2013; 70: 455–461.
9. Pantoni L. Cerebral small vessel disease: from pathogenesis and clinical characteristics to therapeutic challenges. *Lancet Neurol* 2010; 9: 689–701.
10. Wardlaw JM. William M. Feinberg award for excellence in clinical stroke: small vessel disease; a big problem, but fixable. *Stroke*. *Stroke* 2018; 49: 1770–1775.
11. Williams DS, Detre JA, Leigh JS, et al. Magnetic resonance imaging of perfusion using spin inversion of arterial water. *Proc Natl Acad Sci U S A* 1992; 89: 212–216.
12. Asllani I, Habeck C, Borogovac A, et al. Separating function from structure in perfusion imaging of the aging brain. *Hum Brain Mapp* 2009; 30: 2927–2935.
13. Biagi L, Abbruzzese A, Bianchi MC, et al. Age dependence of cerebral perfusion assessed by magnetic resonance continuous arterial spin labeling. *J Magn Reson Imaging* 2007; 25: 696–702.
14. Juttukonda MR, Li B, Alaktoum R, et al. Characterizing cerebral hemodynamics across the adult lifespan with arterial spin labeling MRI data from the human connectome Project-Aging. *Neuroimage* 2021; 230: 117807.
15. Lee C, Lopez OL, Becker JT, et al. Imaging cerebral blood flow in the cognitively normal aging brain with arterial spin labeling: implications for imaging of neurodegenerative disease. *J Neuroimaging* 2009; 19: 344–352.
16. Liu Y, Zhu X, Feinberg D, et al. Arterial spin labeling MRI study of age and gender effects on brain perfusion hemodynamics. *Magn Reson Med* 2012; 68: 912–922.
17. Zhang N, Gordon ML and Goldberg TE. Cerebral blood flow measured by arterial spin labeling MRI at resting state in normal aging and Alzheimer's disease. *Neurosci Biobehav Rev* 2017; 72: 168–175.
18. Dai W, Garcia D, de Bazelaire C, et al. Continuous flow-driven inversion for arterial spin labeling using pulsed radio frequency and gradient fields. *Magn Reson Med* 2008; 60: 1488–1497.

19. Alsop DC, Detre JA, Golay X, et al. Recommended implementation of arterial spin-labeled perfusion MRI for clinical applications: a consensus of the ISMRM perfusion study group and the European consortium for ASL in dementia. *Magn Reson Med* 2015; 73: 102–116.
20. Bahrani AA, Powell DK, Yu G, et al. White matter hyperintensity associations with cerebral blood flow in elderly subjects stratified by cerebrovascular risk. *J Stroke Cerebrovasc Dis* 2017; 26: 779–786.
21. Buijs PC, Krabbe-Hartkamp MJ, Bakker CJ, et al. Effect of age on cerebral blood flow: measurement with ungated two-dimensional phase-contrast MR angiography in 250 adults. *Radiology* 1998; 209: 667–674.
22. Ni L, Zhang B, Yang D, et al. Lower cerebrovascular reactivity contributed to white matter hyperintensity-related cognitive impairment: a resting-state functional MRI study. *J Magn Reson Imaging* 2020; 53: 703–711.
23. Angleys H, Østergaard L and Jespersen SN. The effects of capillary transit time heterogeneity (CTH) on brain oxygenation. *J Cereb Blood Flow Metab* 2015; 35: 806–817.
24. Mouridsen K, Hansen MB, Østergaard L, et al. Reliable estimation of capillary transit time distributions using DSC-MRI. *J Cereb Blood Flow Metab* 2014; 34: 1511–1521.
25. Juttukonda MR, Donahue MJ, Davis LT, et al. Preliminary evidence for cerebral capillary shunting in adults with sickle cell anemia. *J Cereb Blood Flow Metab* 2019; 39: 1099–1110.
26. Juttukonda MR, Donahue MJ, Waddle SL, et al. Reduced oxygen extraction efficiency in sickle cell anemia patients with evidence of cerebral capillary shunting. *J Cereb Blood Flow Metab* 2020; : 271678X20913123.
27. Kim CM, Alvarado RL, Stephens K, et al. Associations between cerebral blood flow and structural and functional brain imaging measures in individuals with neuropsychologically defined mild cognitive impairment. *Neurobiol Aging* 2020; 86: 64–74.
28. Bondi MW, Edmonds EC, Jak AJ, et al. Neuropsychological criteria for mild cognitive impairment improves diagnostic precision, biomarker associations, and progression rates. *J Alzheimers Dis* 2014; 42: 275–289.
29. Dale AM, Fischl B and Sereno MI. Cortical surface-based analysis. I. Segmentation and surface reconstruction. *Neuroimage* 1999; 9: 179–194.
30. Fischl B, Sereno MI and Dale AM. Cortical surface-based analysis. II: inflation, flattening, and a surface-based coordinate system. *Neuroimage* 1999; 9: 195–207.
31. Greve DN and Fischl B. Accurate and robust brain image alignment using boundary-based registration. *Neuroimage* 2009; 48: 63–72.
32. Jenkinson M, Bannister P, Brady M, et al. Improved optimization for the robust and accurate linear registration and motion correction of brain images. *Neuroimage* 2002; 17: 825–841.
33. Donahue MJ, Juttukonda MR and Watchmaker JM. Noise concerns and post-processing procedures in cerebral blood flow (CBF) and cerebral blood volume (CBV) functional magnetic resonance imaging. *Neuroimage* 2017; 154: 43–58.
34. Fan AP, Guo J, Khalighi MM, et al. Long-Delay arterial spin labeling provides more accurate cerebral blood flow measurements in moyamoya patients: a simultaneous positron emission tomography/MRI study. *Stroke* 2017; 48: 2441–2449.
35. Mouridsen K, Friston K, Hjort N, et al. Bayesian estimation of cerebral perfusion using a physiological model of microvasculature. *Neuroimage* 2006; 33: 570–579.
36. Mouridsen K, Christensen S, Gyldensted L, et al. Automatic selection of arterial input function using cluster analysis. *Magn Reson Med* 2006; 55: 524–531.
37. Jespersen SN and Østergaard L. The roles of cerebral blood flow, capillary transit time heterogeneity, and oxygen tension in brain oxygenation and metabolism. *J Cereb Blood Flow Metab* 2012; 32: 264–277.
38. Liu P, Huang H, Rollins N, et al. Quantitative assessment of global cerebral metabolic rate of oxygen (CMRO<sub>2</sub>) in neonates using MRI. *NMR Biomed* 2014; 27: 332–340.
39. Devous MD, Stokely EM, Chehabi HH, et al. Normal distribution of regional cerebral blood flow measured by dynamic single-photon emission tomography. *J Cereb Blood Flow Metab* 1986; 6: 95–104.
40. Hagstadius S and Risberg J. Regional cerebral blood flow characteristics and variations with age in resting normal subjects. *Brain Cogn* 1989; 10: 28–43.
41. Lu H, Xu F, Rodrigue KM, et al. Alterations in cerebral metabolic rate and blood supply across the adult lifespan. *Cereb Cortex* 2011; 21: 1426–1434.
42. Martin AJ, Friston KJ, Colebatch JG, et al. Decreases in regional cerebral blood flow with normal aging. *J Cereb Blood Flow Metab* 1991; 11: 684–689.
43. Frackowiak RS, Lenzi GL, Jones T, et al. Quantitative measurement of regional cerebral blood flow and oxygen metabolism in man using <sup>15</sup>O and positron emission tomography: theory, procedure, and normal values. *J Comput Assist Tomogr* 1980; 4: 727–736.
44. Yamaguchi T, Kanno I, Uemura K, et al. Reduction in regional cerebral metabolic rate of oxygen during human aging. *Stroke* 1986; 17: 1220–1228.
45. Meguro K, Hatazawa J, Yamaguchi T, et al. Cerebral circulation and oxygen metabolism associated with subclinical periventricular hyperintensity as shown by magnetic resonance imaging. *Ann Neurol* 1990; 28: 378–383.
46. Derdeyn CP. Hemodynamics and oxygen extraction in chronic large artery steno-occlusive disease: clinical applications for predicting stroke risk. *J Cereb Blood Flow Metab* 2018; 38: 1584–1597.
47. Watchmaker JM, Juttukonda MR, Davis LT, et al. Hemodynamic mechanisms underlying elevated oxygen extraction fraction (OEF) in moyamoya and sickle cell

- anemia patients. *J Cereb Blood Flow Metab* 2018; 38: 1618–1630.
48. Østergaard L, Jespersen SN, Engedahl T, et al. Capillary dysfunction: its detection and causative role in dementias and stroke. *Curr Neurol Neurosci Rep* 2015; 15: 37.
49. Østergaard L, Engedal TS, Moreton F, et al. Cerebral small vessel disease: capillary pathways to stroke and cognitive decline. *J Cereb Blood Flow Metab* 2016; 36: 302–325.
50. Østergaard L. Blood flow, capillary transit times, and tissue oxygenation: the centennial of capillary recruitment. *J Appl Physiol (1985)* 2020; 129: 1413–1421.
51. Wu X, Ya J, Zhou D, et al. Pathogeneses and imaging features of cerebral white matter lesions of vascular origins. *Aging Dis* 2021; 12: 2031–2051.